Effect of hole-shape irregularities on photonic crystal waveguides

Momchil Minkov[1,*] and Vincenzo Savona[1]

Institute of Theoretical Physics, École Polytechnique Fédérale de Lausanne EPFL, CH-1015 Lausanne, Switzerland
**Corresponding author: momchil.minkov@epfl.ch*

Received April 20, 2012; revised June 13, 2012; accepted June 16, 2012;
posted June 22, 2012 (Doc. ID 166525); published July 20, 2012

The effect of irregular hole shape on the spectrum and radiation losses of a photonic crystal waveguide is studied using Bloch-mode expansion. Deviations from a circular hole are characterized by a radius fluctuation amplitude and correlation angle. It is found that the parameter that determines the magnitude of the effect of disorder is the standard deviation of the hole areas. Hence, for a fixed amplitude of the radius fluctuation around the hole, those effects are strongly dependent on the correlation angle of the irregular shape, which suggests how to potentially improve the quality of photonic crystal structures. © 2012 Optical Society of America

OCIS codes: 230.5298, 220.4241.

Photonic crystals (PHCs) lie at the forefront of research in photonics [1]. One of the main obstacles to the practical implementation of PHCs is disorder originating from the fabrication process. Disorder sets a severe limitation to the quality factor of high-Q PHC cavities [2–4], and degrades the performance of PHC waveguides by inducing extrinsic radiation losses [5–8] and light localization [9] in the vicinity of the guided band edge (which has also been advocated as a useful resource for applications [10]). For these reasons, disorder in PHCs has been the subject of increasingly intense theoretical [2–8,11,12] and experimental [3,4,13–15] studies in the last decade. Several theoretical works [3–5,8,11] have considered the simplest possible disorder model, namely, circular holes with randomly fluctuating radii and/or positions, and studied the spectral properties as a function of the fluctuation amplitude. An analysis based on more realistic assumptions, clarifying the role of the observed deviations from a perfectly circular shape of the PHC holes [13,16], remains a major challenge. Recent experiments [13] have provided strong evidence that the relevant parameter that quantifies the effect of disorder is the amplitude of *fluctuations in the hole area*. On the theoretical side significant progress has been made [2,6,7,12], in particular by estimating the disorder-induced frequency shift of the band edge [12], and by showing that the correlation angle of the hole shape—the measure of how rapidly the radius fluctuates around a hole—strongly affects the loss rates in a PHC waveguide for a fixed amplitude of the radius fluctuations [6]. Yet, the interplay of angle correlation and radius fluctuations, and the relevance of hole-area fluctuations, are still poorly understood.

In this Letter, we address this problem by employing the recently developed [11] Bloch-mode expansion method (BME)—a nonperturbative mode expansion that converges to the exact solution of Maxwell equations within the desired spectral range, but requires a moderate computational effort and allows implementing the hole-shape model of choice in a semianalytical fashion. As a prototypical system, we study a W1-defect waveguide, but our conclusions about the effect of irregular hole shape have a much more general extent. We carry out a systematic analysis for two limiting assumptions within the hole-shape model: fixed radius fluctuation (within each single hole), or fixed hole-area fluctuation (among different holes). The result clearly shows that varying the correlation angle has practically no effect on spectrum and radiation losses in the second case, while it is highly determinant within the first assumption. We conclude by clarifying the mechanism underlying this phenomenology and discuss how it relates to the fabrication process.

The waveguide we consider is based on a triangular lattice of cylindrical holes of radius $R = 0.3a$ in a dielectric slab of thickness $d = 0.5a$, where a is the lattice parameter. The permittivity is set to $\varepsilon_2 = 12.11$ in the dielectric material and to $\varepsilon_1 = 1$ outside. Disorder is modeled in the form of fluctuations in the hole profile, given by $R(\phi) = R + \delta R(\phi)$, where ϕ is the polar angle relative to the hole center. In particular, each hole is characterized by a different disorder realization (no correlation between hole shapes is assumed) defined by random Fourier expansion coefficients C_m as $\delta R(\phi) = \sum_{m=-\infty}^{+\infty} C_m e^{im\phi}$.

The Bloch modes of the regular waveguide are computed via guided-mode expansion [17]. In all computations, we truncate the reciprocal space of guided modes to $G_{\max} = 3(2\pi/a)$ and take a supercell of height $5\sqrt{3}a$ along the direction orthogonal to the waveguide. To apply BME, we need the Fourier transforms of the dielectric profiles of both the regular structure, $\varepsilon(\mathbf{r})$, and the disordered one, $\varepsilon'(\mathbf{r})$. We take the z axis to be orthogonal to the slab plane, in which case both profiles are piecewise constant along z. The only nontrivial task is then the evaluation of the two-dimensional Fourier transforms of $\varepsilon(\boldsymbol{\rho})$ and $\varepsilon'(\boldsymbol{\rho})$ at $z = 0$ inside the slab. The former is readily computed [11], while the latter, to first order in δR, is

$$\varepsilon'(\mathbf{g}) = \varepsilon(\mathbf{g}) + \frac{2\pi R_0(\varepsilon_1 - \varepsilon_2)}{S} \times \sum_{\zeta} e^{i\mathbf{g}\boldsymbol{\rho}_\zeta} \sum_{m=-\infty}^{\infty} i^m e^{im\theta} C_{m,\zeta} J_m(gR_0), \quad (1)$$

where we denote the in-plane position of the center of each hole by $\boldsymbol{\rho}_\zeta$, with ζ running over all holes in the structure, the area of the structure by S, $\mathbf{g} = (g, \theta)$, and the

mth Bessel function of the first kind by $J_m(x)$. Here, we take the $\{C_m\}$ coefficients for each hole to be Gaussian random variables, whose distribution is fully determined by $\langle C_m\rangle$ and $\langle|C_m|^2\rangle$. Note that $\langle C_{m\neq 0}\rangle = 0$, since it is an average over complex numbers with a random phase. We further assume Gaussian correlation along ϕ, such that $\langle\delta R(\phi)\delta R(\phi')\rangle = \sigma^2 e^{-\frac{(\phi-\phi')^2}{2\delta^2}}$, where δ is the correlation angle. We verified that assuming an exponential correlation does not relevantly change our conclusions. This sets $\langle\sum_m |C_m|^2\rangle = \langle\delta R^2\rangle = \sigma^2$, and the dependence with m of the second moments:

$$\langle|C_m|^2\rangle = \sigma^2 \int_{-\pi}^{\pi} e^{-\frac{\phi^2}{2\delta^2}} e^{-im\phi} d\phi. \tag{2}$$

Within this scheme, the quantities σ, δ, and $\langle C_0\rangle$ are still free parameters. To set them, we consider two different models. The first model consists of assuming, for varying δ, a given magnitude of the fluctuation of the hole radius, namely, by setting $\langle\delta R\rangle = 0$ and $\langle\delta R^2\rangle = \text{const}$, which sets $\langle C_0\rangle = 0$ and $\sigma = \sqrt{\langle\delta R^2\rangle}$. Figure 1(a) illustrates one realization of a hole within this model with $\sigma = 0.006a$, computed for two different values of δ. The second model consists, instead, of assuming a given magnitude of the fluctuations in the hole area A, thus setting $\langle\delta A\rangle = 0$ and $\langle\delta A^2\rangle = \text{const}$, which determines implicitly the parameters $\langle C_0\rangle$ and σ. In Fig. 1(c), we show a hole realization when those conditions are imposed, with $\langle\delta A^2\rangle = 0.004a^2$, for the same two values of δ as in Fig. 1(a). It can be seen that, in this case, the magnitude of the radius fluctuations $\langle\delta R^2\rangle$ depends substantially on δ, and while the profile for $\delta = 0.06(2\pi)$ appears as a reasonable representation of what could be expected from a state-of-the-art PHC [13,16], the $\delta = 0.005(2\pi)$ profile displays unrealistically large radius fluctuations.

In Fig. 2, we plot the radiative loss rates and frequencies of the guided modes, computed for one realization of

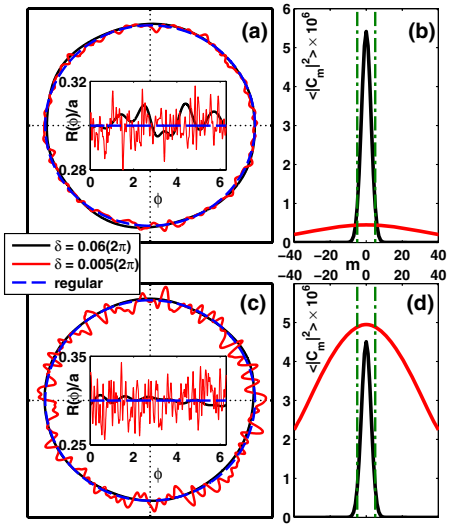

Fig. 1. (Color online) (a) Polar and Cartesian plots of a sample hole shape for two different correlation angles, assuming a fixed radius fluctuation $\sigma = 0.006a$ and (b) the underlying distributions of $\langle|C_m|^2\rangle$. (c) and (d) Same, assuming a fixed area fluctuation $\langle\delta A^2\rangle = 0.004a^2$.

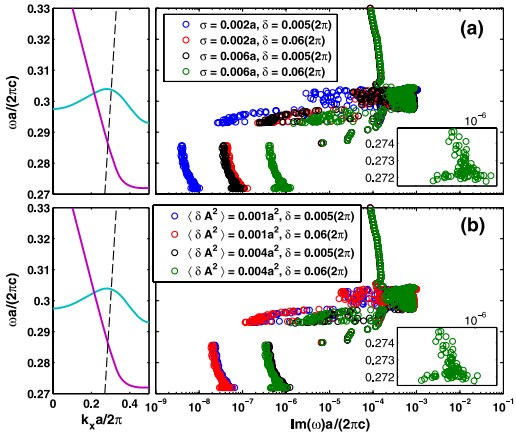

Fig. 2. (Color online) Computed radiation loss rates. (a) $\langle\delta R^2\rangle = \text{const}$ model and (b) $\langle\delta A^2\rangle = \text{const}$ model. Insets: detail of the rates close to the band edge. On the left, the guided bands of the regular structure (solid curves) and the light cone (dashed curve) are displayed for reference.

a waveguide of length $256a$. Radiative rates are computed by assuming perturbative coupling of slab modes to three-dimensional radiative modes, following the prescriptions of [11,17]. It should be noted that these loss rates are computed including the mixing of all Bloch momenta, including those backward-propagating ones that give rise to backscattering losses in a linear response picture [2]. Figure 2(a) represents the fixed-$\langle\delta R^2\rangle$ model, with the four possible combinations of $\delta = 0.06(2\pi)$, $\delta = 0.005(2\pi)$, $\sigma = 0.006a$, and $\sigma = 0.002a$. The magnification in the insets shows the scattering of the rates linked to the randomness. As can be seen, within this model, changing δ can have an effect as dramatic as that of changing σ, with an order of magnitude difference present in the loss rates of the modes when going from the high $\delta = 0.06(2\pi)$ to the low $\delta = 0.005(2\pi)$. In Fig. 2(b), we show a similar plot but for the fixed-$\langle\delta A^2\rangle$ model, with the same two values of δ and with $\langle\delta A^2\rangle = 0.004a^2$ and $\langle\delta A^2\rangle = 0.001a^2$. Here, in contrast, changing δ does not have a very pronounced effect, with the radiative rates being only very slightly higher in the low-δ case. This single-realization data, together with the sample profiles given in Fig. 1, suggest that fine features in the shape of the holes do not contribute as strongly to the disorder effects as do the smooth features.

To test this further, we computed the density of states (DOS) of the modes close to the band edge, by a statistical average over 500 disorder realizations. The computed DOS are plotted in Figs. 3(a) and 3(b) for the fixed-$\langle\delta R^2\rangle$ model and in Figs. 3(c) and 3(d) for the fixed-$\langle\delta A^2\rangle$ one. To emphasize the role of the irregular hole shape, we also plot the DOS with the commonly adopted [3–5,8,11] simple disorder model of constant radius fluctuations (corresponding to the limiting case $\delta \to \infty$). Oscillations in the high-frequency tails originate from the finite length of the simulated waveguide. All the computed histograms show a Lifshitz tail below the band edge. Modes in this region are spatially localized [11,18], and slow-light propagation is consequently hindered [8,14,15]. From the DOS it appears, once more, that the correlation angle δ has a strong effect on the

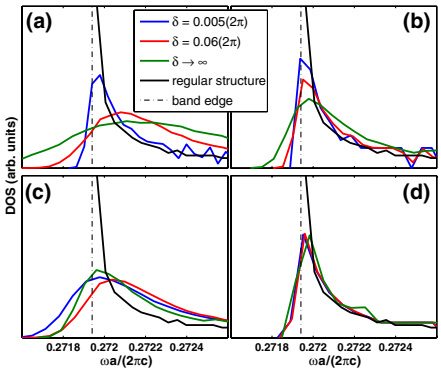

Fig. 3. (Color online) DOS histograms close to the band edge (marked by a dashed–dotted line), for (a) $\sigma = 0.006a$, (b) $\sigma = 0.002a$, (c) $\langle \delta A^2 \rangle = 0.004a^2$, and (d) $\langle \delta A^2 \rangle = 0.001a^2$.

distribution only in the $\langle \delta R^2 \rangle = \text{const}$ case, where the broadening of the band edge increases considerably for increasing δ. In this case, we also expect the parameter δ to affect significantly all effects due to disorder, such as Anderson localization and the breakdown of slow-light propagation.

In all our simulations, the sum in Eq. (1) was restricted to $|m| \le m_{\max}$. We have carefully checked that all results were well converged starting at $m_{\max} = 5$. This remark corroborates our statement that fine features in the disorder are not as relevant as the smooth ones. Intuitively, this is due to the typical wavelength of the electromagnetic modes of the PHC, which produces a spatial averaging of features in the dielectric profile on a much smaller spatial scale.

The main result of this work can be broken down in two statements. First—confirming the suggestion made in a recent experimental study [13]—it is indeed the magnitude of the fluctuations of the hole area, $\langle \delta A^2 \rangle$, that determines the magnitude of the disorder effects. This is evident from Figs. 2 and 3, where a $\langle \delta A^2 \rangle = \text{const}$ model is virtually independent of δ. Second, when $\langle \delta R^2 \rangle = \text{const}$ is imposed instead, the disorder effects are strongly dependent on δ, with a small correlation angle corresponding to much smaller loss rates and spectral broadening. The effect on loss rates was already indicated by a perturbative analysis [6].

Insight is provided by comparing Figs. 1(b) and 1(d), where the average quantities $\langle |C_m|^2 \rangle$ are plotted for the corresponding hole models in Figs. 1(a) and 1(c). The dashed–dotted lines in Figs. 1(b) and 1(d) mark the convergence range $|m| \le m_{\max} = 5$. In the case of fixed radius fluctuation depicted in Fig. 1(b), the values of $\langle |C_m|^2 \rangle$ in this small-$|m|$ range vary considerably when varying δ. This is because the parameters σ and δ determine, respectively, the integral and the width of the distribution $\langle |C_m|^2 \rangle$ as a function of m. In the case of fixed hole-area fluctuations shown in Fig. 1(d) instead, the two curves differ mainly in their width, while their values in the vicinity of $m = 0$ are closer than in the previous case. Thus, for fixed area fluctuations, the C_m coefficients relevant to the results vary less as a function of δ.

The fabrication process of a PHC does not correspond to either of the two limiting models considered in this work. The cross section of the electron beam used for lithography and the subsequent etching process are likely to set a *typical length scale* for the hole shape. For PHCs with nominally constant hole radii, this situation is, however, expected to be closer to the fixed-$\langle \delta R^2 \rangle$ assumption, as Figs. 1(a) and 1(c) also clearly suggest. We conclude that, while hole-area fluctuations are the single relevant parameter for quantifying disorder effects, this parameter is only indirectly determined by the details of the fabrication process, which instead directly set the amplitude of radius fluctuations and their correlation angle. If any control over those two parameters is possible in the fabrication process, then, to increase the PHC quality, we propose minimizing the angular scale of the hole roughness δ, while keeping its amplitude constant. This result provides a valuable indication for further improvement of the quality of PHCs in view of applications in photonics.

References

1. J. D. Joannopoulos, S. G. Johnson, J. N. Winn, and R. D. Meade, *Photonic Crystals: Molding the Flow of Light* (Princeton University, 2008).
2. L. C. Andreani and D. Gerace, Phys. Status Solidi B **244**, 3528 (2007).
3. Y. Taguchi, Y. Takahashi, Y. Sato, T. Asano, and S. Noda, Opt. Express **19**, 11916 (2011).
4. S. L. Portalupi, M. Galli, M. Belotti, L. C. Andreani, T. F. Krauss, and L. O'Faolain, Phys. Rev. B **84**, 045423 (2011).
5. D. Gerace and L. C. Andreani, Opt. Lett. **29**, 1897 (2004).
6. S. Hughes, L. Ramunno, J. F. Young, and J. E. Sipe, Phys. Rev. Lett. **94**, 033903 (2005).
7. M. Patterson, S. Hughes, S. Schulz, D. M. Beggs, T. P. White, L. O'Faolain, and T. F. Krauss, Phys. Rev. B **80**, 195305 (2009).
8. S. Mazoyer, J. P. Hugonin, and P. Lalanne, Phys. Rev. Lett. **103**, 063903 (2009).
9. S. John, Phys. Rev. Lett. **58**, 2486 (1987).
10. L. Sapienza, H. Thyrrestrup, S. Stobbe, P. D. Garcia, S. Smolka, and P. Lodahl, Science **327**, 1352 (2010).
11. V. Savona, Phys. Rev. B **83**, 085301 (2011).
12. M. Patterson and S. Hughes, Phys. Rev. B **81**, 245321 (2010).
13. N. Le Thomas, Z. Diao, H. Zhang, and R. Houdre, J. Vac. Sci. Technol. B **29**, 051601 (2011).
14. S. Mazoyer, P. Lalanne, J. Rodier, J. Hugonin, M. Spasenovi, L. Kuipers, D. Beggs, and T. Krauss, Opt. Express **18**, 14654 (2010).
15. N. Le Thomas, H. Zhang, J. Jágerská, V. Zabelin, R. Houdré, I. Sagnes, and A. Talneau, Phys. Rev. B **80**, 125332 (2009).
16. M. Skorobogatiy, G. Bégin, and A. Talneau, Opt. Express **13**, 2487 (2005).
17. L. C. Andreani and D. Gerace, Phys. Rev. B **73**, 235114 (2006).
18. J. Topolancik, B. Ilic, and F. Vollmer, Phys. Rev. Lett. **99**, 253901 (2007).